

Hund's Rule, Interorbital Hybridization, and High- T_c Superconductivity in the Bilayer Nickelate

Xing-Zhou Qu,^{1,2,*} Dai-Wei Qu,^{1,2,*} Xin-Wei Yi,³ Wei Li,^{2,†} and Gang Su^{2,1,3,‡}

¹*Kavli Institute for Theoretical Sciences, University of Chinese Academy of Sciences, Beijing 100190, China*

²*Institute of Theoretical Physics, Chinese Academy of Sciences, Beijing 100190, China*

³*School of Physical Sciences, University of Chinese Academy of Sciences, Beijing 100049, China*

Understanding the pairing mechanism in bilayer nickelate superconductors constitutes a fascinating quest. Using density matrix renormalization group for $T = 0$ and thermal tensor networks for $T > 0$ properties, along with density functional theory calculations, we investigate the intriguing interplay between the Hund's rule coupling and interorbital hybridization that explains the pressure-dependent high- T_c superconductivity in bilayer nickelates. By studying a two-orbital model, we identify three distinct superconductive (SC) regimes: hybridization dominant, Hund's rule dominant, and the hybrid-Hund synergistic SC regimes. In these SC regimes, both $d_{x^2-y^2}$ and d_{z^2} orbitals exhibit algebraic pairing correlations with similar Luttinger parameters K_{SC} . In particular, the former always exhibits a much stronger amplitude than the latter, with a distinctly higher SC characteristic temperature T_c^* . Below this temperature, the pairing susceptibility diverges as $\chi_{SC}(T) \sim 1/T^{2-K_{SC}}$. With realistic model parameters, we find the pressurized $\text{La}_3\text{Ni}_2\text{O}_7$ falls into the Hund's rule dominated SC regime. As hybridization further enhances under pressure, it leads to significant interorbital frustration and in turn suppresses the SC correlations, explaining the rise and fall of high- T_c superconductivity under high pressure [J. Li, *et al.*, arXiv:2404.11369 (2024)]. Our results offer a comprehensive understanding of the interlayer pairing in superconducting $\text{La}_3\text{Ni}_2\text{O}_7$.

Introduction.— The recent discovery of nearly 80 K superconductive (SC) transition in the pressurized Ruddlesden-Popper perovskite $\text{La}_3\text{Ni}_2\text{O}_7$ [1] has sparked significant research activities in both experiment [2–19] and theory [20–67]. The bilayer structure and orbital selectivity are believed to be key factors in the formation of SC order, and the interlayer antiferromagnetic (AF) coupling is considered as the pairing driving force [33–38, 42, 61]. Nonetheless, debate persists regarding the SC pairing mechanism, particularly with respect to the intriguing roles of Hund's rule coupling and the hybridization between the two e_g orbitals.

The hybridization theory [24, 26, 38, 42, 47, 57, 66, 68–70] considers the interlayer d_{z^2} pairs correlated via the strong interlayer AF coupling. There are few holes in the d_{z^2} orbital, and due to the limited intralayer hopping of d_{z^2} electrons, the preformed pairs necessitate hybridization with itinerant $d_{x^2-y^2}$ orbitals to attain phase coherence [cf., Fig. A1(a)]. Nevertheless, it is unclear whether such SC order in the d_{z^2} orbitals could render high T_c through this mechanism. The significant interlayer t_\perp between d_{z^2} orbitals could result in pronounced Pauli blocking [71]. Together with the small hole density, it weakens the potential SC order within the d_{z^2} orbitals [34, 61, 69], thereby challenging such an SC scenario.

Distinctly, a different scenario suggests that the Hund's rule coupling plays a critical role in forming the high- T_c SC order [33–35, 43, 58, 61, 63]. Although the interlayer spin exchange is quite small in the $d_{x^2-y^2}$ orbitals, the substantial ferromagnetic (FM) Hund's rule coupling $J_H \sim 1$ eV can effectively transfer the interlayer AF coupling from the d_{z^2} to $d_{x^2-y^2}$ orbitals, passing a strong pairing force to the latter [33–35] [cf., Fig. A1(b)]. Moreover, as the quarter-filling $d_{x^2-y^2}$ orbital possesses ample hole density and adequate intralayer hopping amplitude, the SC pairs can thus move coherently within each layer. By integrating out the d_{z^2} orbitals in the large J_H limit and neglecting the interorbital hy-

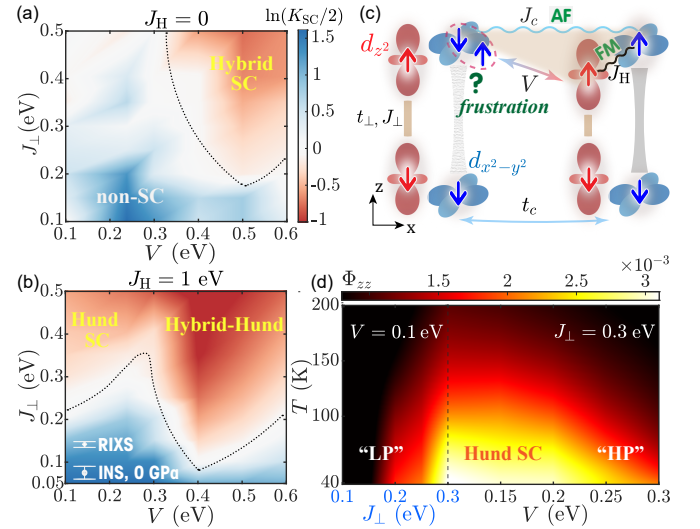


FIG. 1. The ground state J_\perp - V phase diagrams are depicted with (a) $J_H = 0$ and (b) $J_H = 1$ eV, respectively. Other model parameters are fixed according to DFT calculations under about 30 GPa [20]. The dotted lines separating the SC and non-SC regimes are guides for the eye. Three distinct SC regimes include ‘Hybrid’ dominated by V , ‘Hund’ by J_H , and ‘Hybrid-Hund’ by both. Measured J_\perp values from ambient resonant inelastic X-ray scattering (RIXS) [18] and inelastic neutron scattering (INS) [19] experiments are marked in (b). (c) The $d_{x^2-y^2}$ orbital exhibits intralayer couplings (t_c , J_c), while the d_{z^2} orbital features interlayer couplings (t_\perp , J_\perp) and intralayer hopping (t_d). J_H denotes the on-site FM Hund's rule coupling and V represents the interorbital hybridization. The $d_{x^2-y^2}$ - $d_{x^2-y^2}$ superexchange and the $d_{x^2-y^2}$ - d_{z^2} double-exchange-like couplings compete and give rise to interorbital frustration highlighted by the shaded triangle. (d) The contour plot of the interlayer pairing correlation $\Phi_{zz}(r)$ of $d_{x^2-y^2}$ orbital, averaged over $r = 2$ to $L_x/4$.

bridization, a single-orbital t - J - J_\perp model has been proposed, which demonstrates high- T_c superconductivity [33, 34]. This

bilayer pairing mechanism is quite robust and has been discussed before in the context of fermion ladders [72, 73] and bilayer square lattices [74]. Nonetheless, recent experiment finds that the SC order can be suppressed under higher pressure, up to 104 GPa, leading to a right-angled triangular SC phase [15]. Such an observation remains to be explained within the Hund's coupling dominant scenario, and underscores the need for a more comprehensive study incorporating both e_g orbitals of $\text{Ni}^{+2.5}$ in $\text{La}_3\text{Ni}_2\text{O}_7$.

In this study, we consider a bilayer two-orbital model with both Hund's rule coupling and interorbital hybridization, and conduct a comprehensive numerical study. We find that the $d_{x^2-y^2}$ orbital consistently serves as the primary host for ro-

bust SC order, exhibiting stronger algebraic pairing correlations and a higher T_c^* determined from pairing susceptibility compared to those of the d_{z^2} orbitals. We highlight that there are three distinct SC regimes: one dominated by hybridization, another by Hund's rule, and a third by both mechanisms. With realistic parameters, we find the pressurized $\text{La}_3\text{Ni}_2\text{O}_7$ resides in the Hund's SC regime and obtain its finite-temperature phase diagram. Our results explain the non-monotonic pressure-dependent behaviors of SC order observed in recent experiments.

Model and method.— Below we consider the following two-orbital bilayer t - J model

$$\begin{aligned}
 H = & -t_c \sum_{\langle i,j \rangle, \mu, \sigma} \left(c_{i,\mu,\sigma}^\dagger c_{j,\mu,\sigma} + \text{H.c.} \right) + J_c \sum_{\langle i,j \rangle, \mu} \left(\mathbf{S}_{i,\mu}^c \cdot \mathbf{S}_{j,\mu}^c - \frac{1}{4} n_{i,\mu}^c n_{j,\mu}^c \right) \\
 & - t_\perp \sum_{i,\sigma} \left(d_{i,\mu=1,\sigma}^\dagger d_{j,\mu=-1,\sigma} + \text{H.c.} \right) + J_\perp \sum_i \left(\mathbf{S}_{i,\mu=1}^d \cdot \mathbf{S}_{i,\mu=-1}^d - \frac{1}{4} n_{i,\mu=1}^d n_{i,\mu=-1}^d \right) \\
 & - t_d \sum_{\langle i,j \rangle, \mu, \sigma} \left(d_{i,\mu,\sigma}^\dagger d_{j,\mu,\sigma} + \text{H.c.} \right) - V \sum_{\langle i,j \rangle, \mu, \sigma} \left(c_{i,\mu,\sigma}^\dagger d_{j,\mu,\sigma} + \text{H.c.} \right) - J_H \sum_{i,\mu} \mathbf{S}_{i,\mu}^c \cdot \mathbf{S}_{i,\mu}^d + \varepsilon_c \sum_{i,\mu} n_{i,\mu}^c + \varepsilon_d \sum_{i,\mu} n_{i,\mu}^d,
 \end{aligned}$$

where $c_{i,\mu,\sigma}$ ($d_{i,\mu,\sigma}$) denotes the $d_{x^2-y^2}$ (d_{z^2}) electron at site i , layer $\mu = \pm 1$, and spin $\sigma = \{\uparrow, \downarrow\}$. Similarly, spin operators $\mathbf{S}_{i,\mu}^c$ ($\mathbf{S}_{i,\mu}^d$) and density operators $n_{i,\mu}^c$ ($n_{i,\mu}^d$) are defined for the two e_g orbitals. Parameter t_c (t_d) labels the intralayer hopping of the $d_{x^2-y^2}$ (d_{z^2}) orbital. The intralayer spin coupling between the $d_{x^2-y^2}$ electrons is denoted as J_c , while that of d_{z^2} is negligibly small. The interlayer hopping and coupling of the d_{z^2} orbital are labeled as t_\perp and J_\perp , respectively. The interorbital hybridization V and the on-site Hund's rule coupling J_H between the two e_g orbitals are considered, with ε_c and ε_d representing the respective site energies. In the present study, the electron filling is fixed as $3/8$, i.e., $n_e = 1.5$ per site for the two e_g orbitals.

To study the nickelate SC phase, we mainly consider realistic parameters under about 30 GPa, including $t_c = 0.483$ eV, $t_\perp = 0.635$ eV, $t_d = 0.110$ eV, $V = 0.239$ eV, $\varepsilon_c = 0.776$ eV, and $\varepsilon_d = 0.409$ eV [20]. With properly chosen Hubbard $U = 4$ eV [27, 43], the spin couplings are $J_c \simeq 4t_c^2/U = 0.233$ eV and $J_\perp \simeq 4t_\perp^2/U = 0.403$ eV, and the Hund's rule coupling is set as $J_H = 1$ eV ($\sim 2.5J_\perp$) [27, 30, 45]. In the study, we employ DMRG [75–77] for the ground state ($T = 0$) and thermal tensor networks [78–80] for finite-temperature ($T > 0$) calculations. DFT calculations are utilized to obtain coupling parameters under different pressures, especially the hybridization V .

Orbital selectivity and interlayer pairing.— In Fig. 2(a), we show the interlayer correlation $\Phi_{zz}(r) = \langle \Delta_i^\dagger \Delta_j \rangle$, where $\Delta_i^\dagger = \frac{1}{\sqrt{2}} \sum_{\mu=\pm 1} c_{i,\mu,\uparrow}^\dagger c_{i,-\mu,\downarrow}^\dagger$ (for $d_{x^2-y^2}$) and distance $r \equiv |j - i|$. When switched from $d_{x^2-y^2}$ to the d_{z^2} or-

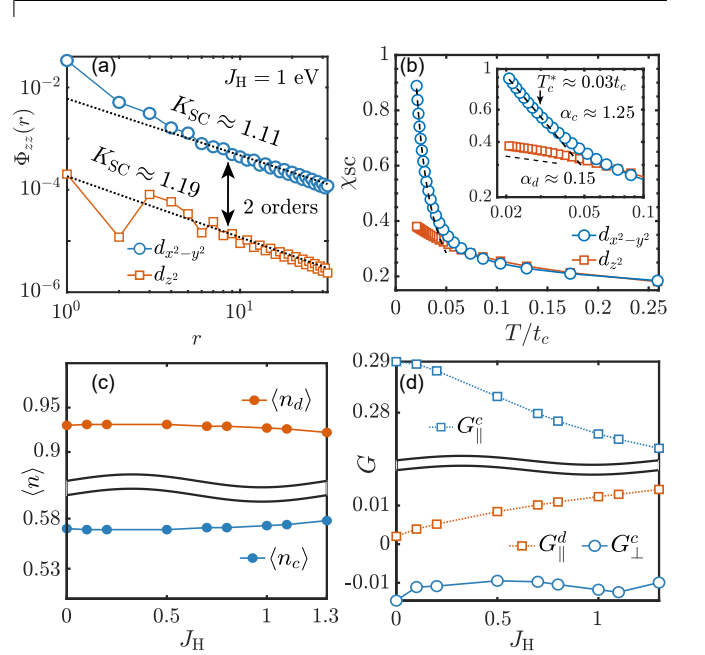


FIG. 2. Pairing correlation $\Phi_{zz}(r)$ and susceptibility χ_{SC} results of bilayer two-orbital model with realistic parameters for $\text{La}_3\text{Ni}_2\text{O}_7$ (see main text). (a) $\Phi_{zz}(r)$ of the $d_{x^2-y^2}$ and d_{z^2} orbitals, with r the distance between two rung pairs. (b) The pairing susceptibility diverges algebraically as $\chi_{\text{SC}} \sim 1/T^{\alpha_c}$ (with $\alpha_c \simeq 1.25$) below $T_c^* \simeq 0.03t_c$ for the $d_{x^2-y^2}$ orbital, while exhibits weak divergence in the d_{z^2} orbital. (c) Electron density and (d) Green's function are calculated in the two e_g orbitals.

bit, we replace $c_{i,\mu,\sigma}$ with $d_{i,\mu,\sigma}$. The pairing suscepti-

bility is defined as $\chi_{\text{SC}}(T) = \frac{1}{L_x} \partial \langle \Delta_{\text{tot}} \rangle_T / \partial h_p$, computed with a small pairing field $h_p = 0.002$ coupled to $\Delta_{\text{tot}} = \frac{1}{2} \sum_{i=\frac{1}{4}L_x}^{\frac{3}{4}L_x} [\Delta_i + (\Delta_i)^\dagger]$ in the bulk of the system. Figure 2(a) presents the pairing correlations $\Phi_{zz}(r)$ for both e_g orbitals, where we find the $d_{x^2-y^2}$ orbital exhibits much stronger pairing correlations, about two orders of magnitude greater than that of the d_{z^2} orbitals. From the power-law fitting, we find the Luttinger parameter $K_{\text{SC}} \simeq 1.11$ for the $d_{x^2-y^2}$ orbital, indicating the presence of (quasi-long range) SC order. Pairing correlations of the d_{z^2} orbital also follow an algebraic scaling with $K_{\text{SC}} \simeq 1.19$. Despite a significant difference — more than an order of magnitude — in pairing correlations between the two e_g orbitals, the proximity effect [58] renders them comparable K_{SC} values.

The small $K_{\text{SC}} \lesssim 1$ implies the divergence of pairing susceptibility. In Fig. 2(b), we show the calculated results of $\chi_{\text{SC}}(T)$ in the two e_g orbitals. In the d_{z^2} orbital, $\chi_{\text{SC}}(T)$ exhibits an increase at lower temperature and shows significantly weaker divergence, thus being secondary in determining the critical temperature T_c . Conversely, the $\chi_{\text{SC}}(T)$ behaviors of the $d_{x^2-y^2}$ orbital suggest $T_c^* \simeq 0.03t_c$, corresponding to a clearly higher transition temperature in the order of 100 K. Moreover, we find the $d_{x^2-y^2}$ orbital exhibits a divergence behavior $\chi_{\text{SC}} \sim 1/T^\alpha$ with an exponent $\alpha \approx 2 - K_{\text{SC}}$, consistent with the determined K_{SC} in the ground-state pairing correlation results.

Figures 2(c,d) show the electron densities $\langle n_{c,d} \rangle$ and the single-particle Green's function $G_{\parallel,\perp}$ in two e_g orbitals. The intralayer Green's function is defined as $G_{\parallel}^\alpha \equiv \frac{1}{2(L_x-1)} \sum_{i,\mu,\sigma} \langle \alpha_{i,\mu,\sigma}^\dagger \alpha_{i+1,\mu,\sigma} \rangle$ between nearest-neighboring (NN) sites within each layer, with $\alpha = \{c, d\}$ denoting orbitals. The interlayer Green's function is defined as $G_{\perp}^c \equiv \frac{1}{L_x} \sum_{i,\sigma} \langle c_{i,\mu=1,\sigma}^\dagger c_{i,\mu=-1,\sigma} \rangle$, reflecting the interlayer electron hopping. The results in Fig. 2(c) indicate that the d_{z^2} orbitals are nearly half-filled with only few holes, in distinction with the approximately quarter-filled $d_{x^2-y^2}$ orbitals with $\langle n_c \rangle \approx 0.58$. In Fig. 2(d), we further point out that the d_{z^2} electrons are rather localized as $G_{\parallel}^d \ll G_{\parallel}^c$, while the $d_{x^2-y^2}$ orbitals are itinerant and can move coherently within each layer (large G_{\parallel}^c), but not across two layers (negligible G_{\perp}^c). In the large J_{H} limit, the single-band t - J - J_{\perp} model [33, 34] can be recovered with strong interlayer pairing.

Hund's SC regime in the two-orbital bilayer model.— In Figs. 1(a,b), we distinguish between SC and non-SC regimes using the fitted Luttinger exponent K_{SC} of the $d_{x^2-y^2}$ orbital. We find a strong interlayer J_{\perp} is crucial for forming a robust SC order in pressurized nickelates. Recent experiments [18, 19] reveal the magnitude of interlayer spin coupling J_{\perp} around 0.1 eV in ambient bulk $\text{La}_3\text{Ni}_2\text{O}_7$, which is located in the non-SC regime [cf., Fig. 1(b)]. The influence of other parameters like the intralayer hopping t_c are relatively small, as demonstrated in the Appendix.

As shown in Figs. 1(a,b), we identify three distinct SC regimes, namely, the ‘‘Hybrid SC’’ regime dominated by hybridization V , ‘‘Hund's SC’’ regime with strong coupling J_{H} ,

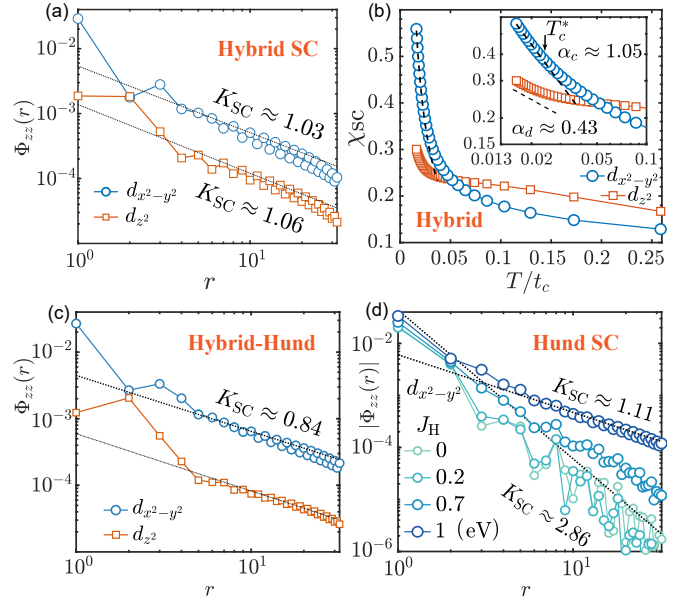


FIG. 3. (a) Pairing correlation Φ_{zz} and (b) finite-temperature pairing susceptibilities of the $d_{x^2-y^2}$ and d_{z^2} orbitals within the hybridization SC regime ($J_{\text{H}} = 0$, $V = 0.5$ eV). Same correlations are shown for the (c) Hybrid-Hund ($J_{\text{H}} = 1$ eV, $V = 0.5$ eV) and (d) Hund's SC regime ($V = 0.239$ eV), where the Hund's rule coupling J_{H} varies from zero to 1 eV.

and the integrated ‘‘Hybrid-Hund SC’’ regime where both couplings are essential and synergistic. In Fig. 3(a), we show that $\Phi_{zz}(r) \sim r^{-K_{\text{SC}}}$ with $K_{\text{SC}} \approx 1.03$ for the $d_{x^2-y^2}$ orbital at $V = 0.5$ eV. In Fig. 3(b), we uncover that the SC pairing susceptibility χ_{SC} of the $d_{x^2-y^2}$ orbital adheres to a scaling law of $1/T^{\alpha_c}$, where $\alpha_c \approx 2 - K_{\text{SC}}$. Notably, the d_{z^2} orbital also demonstrates a comparable Luttinger parameter of $K_{\text{SC}} \approx 1$; however, these correlations are substantially weaker in intensity. Consequently, even within the hybrid SC scenario, the d_{z^2} orbital pairing arises primarily through a proximity-induced mechanism rather than being the dominant contributor.

In Fig. 1(b), there exists a hybrid-Hund SC regime where both V and J_{H} cooperate to render a robust SC order. In Fig. 3(c), we set $J_{\text{H}} = 1$ eV and introduce large $V = 0.5$ eV, finding that the interlayer pairing correlations for both orbitals exhibit power-law scaling with $K_{\text{SC}} \approx 0.84$. Nevertheless, the much larger amplitude ensures again the dominance of SC pairing with the $d_{x^2-y^2}$ electrons. Although the hybrid and hybrid-Hund SC regimes can have $K_{\text{SC}} \lesssim 2$, the required hybridization $V \gtrsim 0.4$ eV exceeds realistic value in the compound $\text{La}_3\text{Ni}_2\text{O}_7$.

Within a realistic range of V , we demonstrate in Fig. 1(b) a SC regime where Hund's rule coupling J_{H} plays a dominant role. In Fig. 3(d), with fixed $V = 0.239$ eV and increasing J_{H} , we find the SC pairing correlation gradually enhances and a quasi-long-range order develops. The results with $J_{\text{H}} = 1$ eV are plotted again here as a reference. Therefore, we conclude that the pressurized $\text{La}_3\text{Ni}_2\text{O}_7$ is located within the Hund's

SC regime, and J_H is essential for driving the SC pairing.

Pressure evolution of the SC order.— High- T_c SC emerges in $\text{La}_3\text{Ni}_2\text{O}_7$ [1, 15] under moderately high pressure above 15 GPa; however, further increasing the pressure suppresses rather than enhances the SC order [15]. Such a non-monotonic behavior can be captured by our two-orbital model.

Following a significant enhancement in J_\perp due to the pressure-induced structural transition [29, 45, 53, 59], the system shifts upwards in the phase diagram, thereby entering the Hund’s SC regime [see Fig. 1(b)]. However, further increases in pressure can lead to substantial hybridization (V) [see Fig. 4(a)], causing deviation from the Hund’s regime and suppression of the SC order. Within such a scenario, the overall two-step pressure evolution is depicted in Fig. 1(d), where we show the interlayer $d_{x^2-y^2}$ pairing correlations $\Phi_{zz}(r)$ averaged from $r = 2$ to $L_x/4$. From low-pressure (“LP”) to high-pressure (“HP”) regime, the increased interlayer spin coupling J_\perp renders the emergence of high- T_c SC. Nevertheless, further increasing pressure would enhance V , leading to the suppression of SC order gradually in the over-pressurized regime. Our results provide a possible explanation of the reported pressure-temperature phase diagram in recent experiments [15].

Suppression of SC order and interorbital frustration.— To uncover the coupling parameters at varying pressure levels, we employ DFT calculations. These calculations reveal the presence of an AF order in the magnetic ground state of $\text{La}_3\text{Ni}_2\text{O}_7$ [81], as opposed to a nonmagnetic (NM) configuration. In addition, strong Fermi surface nesting can also induce charge density wave (CDW) instability [81]. For each configuration depicted in Fig. 4(b), we perform Wannier downfolding of the DFT band structure to obtain the hopping parameters of the bilayer two-orbital model (see Appendix for details). Similar analysis is also performed for Pr-doped $\text{La}_2\text{PrNi}_2\text{O}_7$ with the NM configuration, with the obtained hybridization V shown in Fig. 4(a). These results show that V increases from ~ 0.15 eV to ~ 0.33 eV with pressure in both compounds.

In Fig. 4(c), we illustrate the influence of V on the SC order by examining the behaviors of K_{SC} . For $J_\perp = 0.25$ eV and 0.3 eV, K_{SC} becomes greater than 2 as $V \gtrsim 0.3$ eV, which corresponds to about 100 GPa pressure in experiment [cf., Fig. 4(a)]. The system thus leaves the Hund’s SC regime due to the enhancement of V in Fig. 1(b). We attribute the suppression of SC order to the magnetic frustration effect illustrated in Fig. 1(c). This effect intensifies as pressure — and particularly V — increases, leading to weakened interlayer AF correlations as well as SC pairing between $d_{x^2-y^2}$ orbitals.

To better quantify the interorbital frustration, we compute the interlayer $d_{x^2-y^2}$ spin correlation F_\perp^c and intralayer correlations $F_\parallel^{\alpha,\alpha'} \equiv \frac{1}{2(L_x-1)} \sum_{i,\mu} \langle \mathbf{S}_{i,\mu}^\alpha \cdot \mathbf{S}_{i+1,\mu}^{\alpha'} \rangle$, where $\alpha, \alpha' \in \{c, d\}$ denote the two orbitals. As depicted in Fig. 4(d), within the Hund’s SC regime, the intralayer spin correlation between the $d_{x^2-y^2}$ orbitals is dominated by the intralayer super-exchange $J_c > 0$. As V increases, the FM corre-

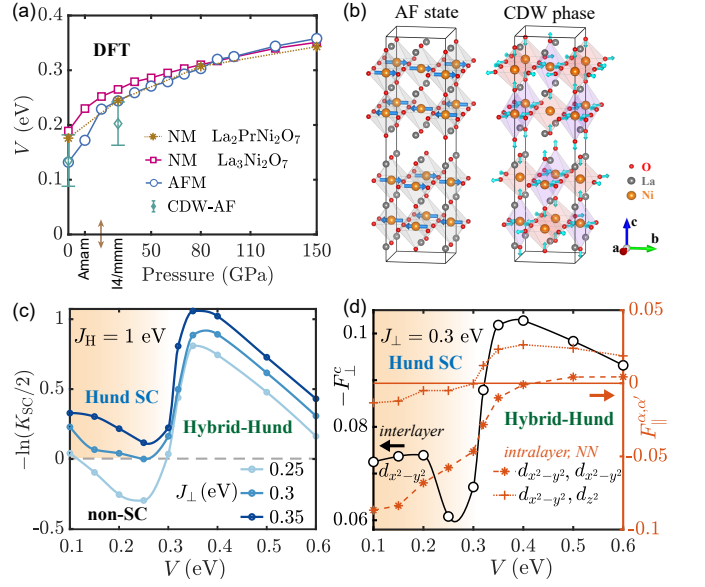


FIG. 4. (a) DFT results for the pristine and CDW phases with both NM and AF configurations as illustrated in (b). For the CDW-AF phase, error bars in the hybridization V reflect its non-uniform distribution due to oxygen octahedra distortion. The ambient and 10 GPa data are obtained from $Amam$ phase while others are from $I4/mmm$ phase. (c) The SC Luttinger parameters K_{SC} and (d) the interlayer spin correlation $-F_\perp^c$ and intralayer $F_\parallel^{\alpha,\alpha'}$ ($\alpha, \alpha' \in \{c, d\}$) between NN sites are plotted. J_H is fixed as 1 eV in the calculations.

lation strengthens due to the differing electron fillings between the two orbitals and the presence of Hund’s rule coupling, which together facilitate a double-exchange-like FM coupling. The competition between AF super-exchange and FM double-exchange couplings introduces interorbital frustration to the system, leading to a switch in intralayer spin correlations from AF to FM. As shown in Fig. 4(d), the strength of the interlayer AF correlation $|F_\perp^c|$ also decreases, weakening the interlayer pairing. Upon further enhancing the hybridization V to overcome the AF $J_c > 0$, spin frustration becomes alleviated in the hybrid-Hund regime. Consequently in the hybrid-Hund regime, V and J_H cooperate and stabilize a robust SC order.

Discussion and outlook.— In this work, we perform a comprehensive numerical study of the bilayer two-orbital t - J model, with both interorbital hybridization and Hund’s rule coupling included and treated on equal footing. With realistic model parameters, we find the pressurized $\text{La}_3\text{Ni}_2\text{O}_7$ resides in the Hund’s rule dominated regime, in which the $d_{x^2-y^2}$ orbital is mainly responsible for forming the SC order, while the d_{z^2} orbital becomes superconducting via the proximity effect. Furthermore, in the finite-temperature phase diagram, we find that increasing pressure can suppress the SC order, which explains the very recently observed right-triangle SC phase in $\text{La}_3\text{Ni}_2\text{O}_7$ [15]. Besides $\text{La}_3\text{Ni}_2\text{O}_7$, we expect similar SC behaviors in $\text{La}_2\text{PrNi}_2\text{O}_7$ under high pressure [2, 17].

Our two-orbital model not only explains the emergent SC order in the pressurized bulk but can also be suggestive for the

ultrathin films [3, 82]. In bulk materials, a structural transition occurs from orthorhombic to tetragonal crystal structure [1, 15]. This transition is accompanied by a significant increase in interlayer AF coupling, which stabilizes the SC order. In thin films, such high-symmetry tetragonal phase is proposed to be stabilized by strain and exists even at ambient pressure [82]. According to our two-orbital scenario dominated by Hund's rule, the enhanced interlayer AF coupling likely accounts for the observed high- T_c superconductivity. When the $d_{x^2-y^2}$ orbital approaches half filling, this would be beneficial rather than detrimental (see Fig. A3) to the robust SC order.

To differentiate between the Hund's rule and hybrid-Hund scenarios, we propose that it is essential to measure the intralayer spin correlations. As depicted in Fig. 4(d), the Hund's SC regime features AF correlations due to the $d_{x^2-y^2} - d_{x^2-y^2}$ super-exchange coupling. Distinctly, in the hybrid-Hund regime, significant V greatly enhances FM double-exchange coupling, and the interplay between the two drives the rise and fall of SC order in $\text{La}_3\text{Ni}_2\text{O}_7$. Therefore, further magnetic measurements on the SC phase are necessary to gain insights into the pairing mechanism, which becomes experimentally accessible very recently with ultrathin $\text{La}_3\text{Ni}_2\text{O}_7$ films [3, 82].

Acknowledgments.— The authors are indebted to Jialin Chen, Qiaoyi Li, Xian-Xin Wu, Rong Yu, Fan Yang, and Congjun Wu for stimulating discussions. This work was supported by the National Natural Science Foundation of China (Grant Nos. 12222412 and 12047503), Innovation Program for Quantum Science and Technology (Nos. 2021ZD0301800 and 2021ZD0301900), and CAS Project for Young Scientists in Basic Research (Grant No. YSBR-057). We thank the HPC-ITP for the technical support and generous allocation of CPU time.

* These authors contributed equally to this work.

† w.li@itp.ac.cn

‡ sugang@itp.ac.cn

- [1] H. Sun, M. Huo, X. Hu, J. Li, Z. Liu, Y. Han, L. Tang, Z. Mao, P. Yang, B. Wang, J. Cheng, D.-X. Yao, G.-M. Zhang, and M. Wang, Signatures of superconductivity near 80 K in a nickelate under high pressure, *Nature* **621**, 493 (2023).
- [2] N. Wang, G. Wang, X. Shen, J. Hou, J. Luo, X. Ma, H. Yang, L. Shi, J. Dou, J. Feng, J. Yang, Y. Shi, Z. Ren, H. Ma, P. Yang, Z. Liu, Y. Liu, H. Zhang, X. Dong, Y. Wang, K. Jiang, J. Hu, S. Nagasaki, K. Kitagawa, S. Calder, J. Yan, J. Sun, B. Wang, R. Zhou, Y. Uwatoko, and J. Cheng, Bulk high-temperature superconductivity in pressurized tetragonal $\text{La}_2\text{PrNi}_2\text{O}_7$, *Nature* **634**, 579 (2024).
- [3] E. K. Ko, Y. Yu, Y. Liu, L. Bhatt, J. Li, V. Thampy, C.-T. Kuo, B. Y. Wang, Y. Lee, K. Lee, J.-S. Lee, B. H. Goodge, D. A. Muller, and H. Y. Hwang, Signatures of ambient pressure superconductivity in thin film $\text{La}_3\text{Ni}_2\text{O}_7$, *Nature* **10.1038/s41586-024-08525-3** (2024).
- [4] Z. Liu, M. Huo, J. Li, Q. Li, Y. Liu, Y. Dai, X. Zhou, J. Hao, Y. Lu, M. Wang, and H.-H. Wen, Electronic correlations and partial gap in the bilayer nickelate $\text{La}_3\text{Ni}_2\text{O}_7$, *Nature Commun-*
- ications* **15**, 7570 (2024).
- [5] J. Hou, P.-T. Yang, Z.-Y. Liu, J.-Y. Li, P.-F. Shan, L. Ma, G. Wang, N.-N. Wang, H.-Z. Guo, J.-P. Sun, Y. Uwatoko, M. Wang, G.-M. Zhang, B.-S. Wang, and J.-G. Cheng, Emergence of High-Temperature Superconducting Phase in Pressurized $\text{La}_3\text{Ni}_2\text{O}_7$ Crystals, *Chinese Physics Letters* **40**, 117302 (2023).
- [6] Y. Zhang, D. Su, Y. Huang, Z. Shan, H. Sun, M. Huo, K. Ye, J. Zhang, Z. Yang, Y. Xu, Y. Su, R. Li, M. Smidman, M. Wang, L. Jiao, and H. Yuan, High-temperature superconductivity with zero resistance and strange-metal behaviour in $\text{La}_3\text{Ni}_2\text{O}_{7-\delta}$, *Nature Physics* **20**, 1269 (2024).
- [7] J. Yang, H. Sun, X. Hu, Y. Xie, T. Miao, H. Luo, H. Chen, B. Liang, W. Zhu, G. Qu, C.-Q. Chen, M. Huo, Y. Huang, S. Zhang, F. Zhang, F. Yang, Z. Wang, Q. Peng, H. Mao, G. Liu, Z. Xu, T. Qian, D.-X. Yao, M. Wang, L. Zhao, and X. J. Zhou, Orbital-dependent electron correlation in double-layer nickelate $\text{La}_3\text{Ni}_2\text{O}_7$, *Nature Communications* **15**, 4373 (2024).
- [8] M. Zhang, C. Pei, Q. Wang, Y. Zhao, C. Li, W. Cao, S. Zhu, J. Wu, and Y. Qi, Effects of pressure and doping on Ruddlesden-Popper phases $\text{La}_{n+1}\text{Ni}_n\text{O}_{3n+1}$, *Journal of Materials Science & Technology* **185**, 147 (2024).
- [9] G. Wang, N. N. Wang, X. L. Shen, J. Hou, L. Ma, L. F. Shi, Z. A. Ren, Y. D. Gu, H. M. Ma, P. T. Yang, Z. Y. Liu, H. Z. Guo, J. P. Sun, G. M. Zhang, S. Calder, J.-Q. Yan, B. S. Wang, Y. Uwatoko, and J.-G. Cheng, Pressure-Induced Superconductivity In Polycrystalline $\text{La}_3\text{Ni}_2\text{O}_{7-\delta}$, *Phys. Rev. X* **14**, 011040 (2024).
- [10] G. Wang, N. Wang, Y. Wang, L. Shi, X. Shen, J. Hou, H. Ma, P. Yang, Z. Liu, H. Zhang, X. Dong, J. Sun, B. Wang, K. Jiang, J. Hu, Y. Uwatoko, and J. Cheng, Observation of high-temperature superconductivity in the high-pressure tetragonal phase of $\text{La}_2\text{PrNi}_2\text{O}_{7-\delta}$ (2023), [arXiv:2311.08212](https://arxiv.org/abs/2311.08212) [cond-mat.supr-con].
- [11] T. Cui, S. Choi, T. Lin, C. Liu, G. Wang, N. Wang, S. Chen, H. Hong, D. Rong, Q. Wang, Q. Jin, J.-O. Wang, L. Gu, C. Ge, C. Wang, J.-G. Cheng, Q. Zhang, L. Si, K.-j. Jin, and E.-J. Guo, Strain-mediated phase crossover in Ruddlesden-Popper nickelates, *Communications Materials* **5**, 32 (2024).
- [12] K. Chen, X. Liu, J. Jiao, M. Zou, C. Jiang, X. Li, Y. Luo, Q. Wu, N. Zhang, Y. Guo, and L. Shu, Evidence of Spin Density Waves in $\text{La}_3\text{Ni}_2\text{O}_{7-\delta}$, *Phys. Rev. Lett.* **132**, 256503 (2024).
- [13] U. Kumar, C. Melnick, and G. Kotliar, Softening of dd excitation in the resonant inelastic x-ray scattering spectra as a signature of Hund's coupling in nickelates (2023), [arXiv:2310.00983](https://arxiv.org/abs/2310.00983) [cond-mat.str-el].
- [14] Z. Dong, M. Huo, J. Li, J. Li, P. Li, H. Sun, L. Gu, Y. Lu, M. Wang, Y. Wang, and Z. Chen, Visualization of oxygen vacancies and self-doped ligand holes in $\text{La}_3\text{Ni}_2\text{O}_{7-\delta}$, *Nature* **630**, 847 (2024).
- [15] J. Li, P. Ma, H. Zhang, X. Huang, C. Huang, M. Huo, D. Hu, Z. Dong, C. He, J. Liao, X. Chen, T. Xie, H. Sun, and M. Wang, Pressure-driven right-triangle shape superconductivity in bilayer nickelate $\text{La}_3\text{Ni}_2\text{O}_7$ (2024), [arXiv:2404.11369](https://arxiv.org/abs/2404.11369) [cond-mat.supr-con].
- [16] Y. Liu, M. Ou, H. Chu, H. Yang, Q. Li, Y. Zhang, and H.-H. Wen, Growth and characterization of the $\text{La}_3\text{Ni}_2\text{O}_{7-\delta}$ thin films: dominant contribution of the $d_{x^2-y^2}$ orbital at ambient pressure (2024), [arXiv:2406.08789](https://arxiv.org/abs/2406.08789) [cond-mat.supr-con].
- [17] J. Wen, Y. Xu, G. Wang, Z.-X. He, Y. Chen, N. Wang, T. Lu, X. Ma, F. Jin, L. Chen, M. Liu, J.-W. Fan, X. Liu, X.-Y. Pan, G.-Q. Liu, J. Cheng, and X. Yu, Probing the Meissner effect in pressurized bilayer nickelate superconductors using diamond quantum sensors (2024), [arXiv:2410.10275](https://arxiv.org/abs/2410.10275) [cond-

mat.supr-con].

- [18] X. Chen, J. Choi, Z. Jiang, J. Mei, K. Jiang, J. Li, S. Agrestini, M. Garcia-Fernandez, H. Sun, X. Huang, D. Shen, M. Wang, J. Hu, Y. Lu, K.-J. Zhou, and D. Feng, Electronic and magnetic excitations in $\text{La}_3\text{Ni}_2\text{O}_7$, *Nature Communications* **15**, 9597 (2024).
- [19] T. Xie, M. Huo, X. Ni, F. Shen, X. Huang, H. Sun, H. C. Walker, D. Adroja, D. Yu, B. Shen, L. He, K. Cao, and M. Wang, Strong interlayer magnetic exchange coupling in $\text{La}_3\text{Ni}_2\text{O}_{7-\delta}$ revealed by inelastic neutron scattering, *Science Bulletin* **69**, 3221 (2024).
- [20] Z. Luo, X. Hu, M. Wang, W. Wú, and D.-X. Yao, Bilayer Two-Orbital Model of $\text{La}_3\text{Ni}_2\text{O}_7$ under Pressure, *Phys. Rev. Lett.* **131**, 126001 (2023).
- [21] Y. Zhang, L.-F. Lin, A. Moreo, and E. Dagotto, Electronic structure, dimer physics, orbital-selective behavior, and magnetic tendencies in the bilayer nickelate superconductor $\text{La}_3\text{Ni}_2\text{O}_7$ under pressure, *Phys. Rev. B* **108**, L180510 (2023).
- [22] Q.-G. Yang, D. Wang, and Q.-H. Wang, Possible s_{\pm} -wave superconductivity in $\text{La}_3\text{Ni}_2\text{O}_7$, *Phys. Rev. B* **108**, L140505 (2023).
- [23] F. Lechnermann, J. Gondolf, S. Bötzel, and I. M. Eremin, Electronic correlations and superconducting instability in $\text{La}_3\text{Ni}_2\text{O}_7$ under high pressure, *Phys. Rev. B* **108**, L201121 (2023).
- [24] H. Sakakibara, N. Kitamine, M. Ochi, and K. Kuroki, Possible High T_c Superconductivity in $\text{La}_3\text{Ni}_2\text{O}_7$ under High Pressure through Manifestation of a Nearly Half-Filled Bilayer Hubbard Model, *Phys. Rev. Lett.* **132**, 106002 (2024).
- [25] Y. Gu, C. Le, Z. Yang, X. Wu, and J. Hu, Effective model and pairing tendency in bilayer Ni-based superconductor $\text{La}_3\text{Ni}_2\text{O}_7$ (2023), [arXiv:2306.07275](https://arxiv.org/abs/2306.07275) [cond-mat.supr-con].
- [26] Y. Shen, M. Qin, and G.-M. Zhang, Effective Bi-Layer Model Hamiltonian and Density-Matrix Renormalization Group Study for the High- T_c Superconductivity in $\text{La}_3\text{Ni}_2\text{O}_7$ under High Pressure, *Chinese Physics Letters* **40**, 127401 (2023).
- [27] V. Christiansson, F. Petocchi, and P. Werner, Correlated Electronic Structure of $\text{La}_3\text{Ni}_2\text{O}_7$ under Pressure, *Phys. Rev. Lett.* **131**, 206501 (2023).
- [28] D. A. Shilenko and I. V. Leonov, Correlated electronic structure, orbital-selective behavior, and magnetic correlations in double-layer $\text{La}_3\text{Ni}_2\text{O}_7$ under pressure, *Phys. Rev. B* **108**, 125105 (2023).
- [29] W. Wú, Z. Luo, D.-X. Yao, and M. Wang, Superexchange and charge transfer in the nickelate superconductor $\text{La}_3\text{Ni}_2\text{O}_7$ under pressure, *Science China Physics, Mechanics & Astronomy* **67**, 117402 (2024).
- [30] Y. Cao and Y.-f. Yang, Flat bands promoted by Hund's rule coupling in the candidate double-layer high-temperature superconductor $\text{La}_3\text{Ni}_2\text{O}_7$ under high pressure, *Phys. Rev. B* **109**, L081105 (2024).
- [31] X. Chen, P. Jiang, J. Li, Z. Zhong, and Y. Lu, Critical charge and spin instabilities in superconducting $\text{La}_3\text{Ni}_2\text{O}_7$ (2023), [arXiv:2307.07154](https://arxiv.org/abs/2307.07154) [cond-mat.supr-con].
- [32] Y.-B. Liu, J.-W. Mei, F. Ye, W.-Q. Chen, and F. Yang, s^{\pm} -Wave Pairing and the Destructive Role of Apical-Oxygen Deficiencies in $\text{La}_3\text{Ni}_2\text{O}_7$ under Pressure, *Phys. Rev. Lett.* **131**, 236002 (2023).
- [33] C. Lu, Z. Pan, F. Yang, and C. Wu, Interlayer-Coupling-Driven High-Temperature Superconductivity in $\text{La}_3\text{Ni}_2\text{O}_7$ under Pressure, *Phys. Rev. Lett.* **132**, 146002 (2024).
- [34] X.-Z. Qu, D.-W. Qu, J. Chen, C. Wu, F. Yang, W. Li, and G. Su, Bilayer $t-J-J_{\perp}$ Model and Magnetically Mediated Pairing in the Pressurized Nickelate $\text{La}_3\text{Ni}_2\text{O}_7$, *Phys. Rev. Lett.* **132**, 036502 (2024).
- [35] H. Oh and Y.-H. Zhang, Type-II $t - J$ model and shared superexchange coupling from Hund's rule in superconducting $\text{La}_3\text{Ni}_2\text{O}_7$, *Phys. Rev. B* **108**, 174511 (2023).
- [36] Y. Zhang, L.-F. Lin, A. Moreo, T. A. Maier, and E. Dagotto, Structural phase transition, s_{\pm} -wave pairing, and magnetic stripe order in bilayered superconductor $\text{La}_3\text{Ni}_2\text{O}_7$ under pressure, *Nature Communications* **15**, 2470 (2024).
- [37] Z. Liao, L. Chen, G. Duan, Y. Wang, C. Liu, R. Yu, and Q. Si, Electron correlations and superconductivity in $\text{La}_3\text{Ni}_2\text{O}_7$ under pressure tuning, *Phys. Rev. B* **108**, 214522 (2023).
- [38] Y.-f. Yang, G.-M. Zhang, and F.-C. Zhang, Interlayer valence bonds and two-component theory for high- T_c superconductivity of $\text{La}_3\text{Ni}_2\text{O}_7$ under pressure, *Phys. Rev. B* **108**, L201108 (2023).
- [39] K. Jiang, Z. Wang, and F.-C. Zhang, High-Temperature Superconductivity in $\text{La}_3\text{Ni}_2\text{O}_7$, *Chin. Phys. Lett.* **41**, 017402 (2024).
- [40] Y. Zhang, L.-F. Lin, A. Moreo, T. A. Maier, and E. Dagotto, Trends in electronic structures and s_{\pm} -wave pairing for the rare-earth series in bilayer nickelate superconductor $R_3\text{Ni}_2\text{O}_7$, *Phys. Rev. B* **108**, 165141 (2023).
- [41] J. Huang, Z. D. Wang, and T. Zhou, Impurity and vortex states in the bilayer high-temperature superconductor $\text{La}_3\text{Ni}_2\text{O}_7$, *Phys. Rev. B* **108**, 174501 (2023).
- [42] Q. Qin and Y.-f. Yang, High- T_c superconductivity by mobilizing local spin singlets and possible route to higher T_c in pressurized $\text{La}_3\text{Ni}_2\text{O}_7$, *Phys. Rev. B* **108**, L140504 (2023).
- [43] Y.-H. Tian, Y. Chen, J.-M. Wang, R.-Q. He, and Z.-Y. Lu, Correlation effects and concomitant two-orbital s_{\pm} -wave superconductivity in $\text{La}_3\text{Ni}_2\text{O}_7$ under high pressure, *Phys. Rev. B* **109**, 165154 (2024).
- [44] D.-C. Lu, M. Li, Z.-Y. Zeng, W. Hou, J. Wang, F. Yang, and Y.-Z. You, Superconductivity from Doping Symmetric Mass Generation Insulators: Application to $\text{La}_3\text{Ni}_2\text{O}_7$ under Pressure (2023), [arXiv:2308.11195](https://arxiv.org/abs/2308.11195) [cond-mat.str-el].
- [45] R. Jiang, J. Hou, Z. Fan, Z.-J. Lang, and W. Ku, Pressure Driven Fractionalization of Ionic Spins Results in Cupratelike High- T_c Superconductivity in $\text{La}_3\text{Ni}_2\text{O}_7$, *Phys. Rev. Lett.* **132**, 126503 (2024).
- [46] N. Kitamine, M. Ochi, and K. Kuroki, Theoretical designing of multiband Nickelate and Palladate superconductors with $d^{8+\delta}$ configuration (2023), [arXiv:2308.12750](https://arxiv.org/abs/2308.12750) [cond-mat.supr-con].
- [47] Z. Luo, B. Lv, M. Wang, W. Wú, and D.-X. Yao, High- T_c superconductivity in $\text{La}_3\text{Ni}_2\text{O}_7$ based on the bilayer two-orbital t - J model, *npj Quantum Materials* **9**, 61 (2024).
- [48] J.-X. Zhang, H.-K. Zhang, Y.-Z. You, and Z.-Y. Weng, Strong Pairing Originated from an Emergent \mathbb{Z}_2 Berry Phase in $\text{La}_3\text{Ni}_2\text{O}_7$, *Phys. Rev. Lett.* **133**, 126501 (2024).
- [49] Z. Pan, C. Lu, F. Yang, and C. Wu, Effect of Rare-Earth Element Substitution in Superconducting $R_3\text{Ni}_2\text{O}_7$ under Pressure, *Chinese Physics Letters* **41**, 087401 (2024).
- [50] H. Sakakibara, M. Ochi, H. Nagata, Y. Ueki, H. Sakurai, R. Matsumoto, K. Terashima, K. Hirose, H. Ohta, M. Kato, Y. Takano, and K. Kuroki, Theoretical analysis on the possibility of superconductivity in the trilayer Ruddlesden-Popper nickelate $\text{La}_4\text{Ni}_3\text{O}_{10}$ under pressure and its experimental examination: Comparison with $\text{La}_3\text{Ni}_2\text{O}_7$, *Phys. Rev. B* **109**, 144511 (2024).
- [51] H. Lange, L. Homeier, E. Demler, U. Schollwöck, A. Bohrdt, and F. Grusdt, Pairing dome from an emergent Feshbach resonance in a strongly repulsive bilayer model, *Phys. Rev. B* **110**, L081113 (2024).
- [52] B. Geisler, J. J. Hamlin, G. R. Stewart, R. G. Hennig, and P. J. Hirschfeld, Structural transitions, octahedral rotations, and

- electronic properties of $A_3Ni_2O_7$ rare-earth nickelates under high pressure, *npj Quantum Materials* **9**, 38 (2024).
- [53] H. Yang, H. Oh, and Y.-H. Zhang, Strong pairing from a small Fermi surface beyond weak coupling: Application to $La_3Ni_2O_7$, *Phys. Rev. B* **110**, 104517 (2024).
- [54] L. C. Rhodes and P. Wahl, Structural routes to stabilize superconducting $La_3Ni_2O_7$ at ambient pressure, *Phys. Rev. Mater.* **8**, 044801 (2024).
- [55] H. Lange, L. Homeier, E. Demler, U. Schollwöck, F. Grusdt, and A. Bohrdt, Feshbach resonance in a strongly repulsive ladder of mixed dimensionality: A possible scenario for bilayer nickelate superconductors, *Phys. Rev. B* **109**, 045127 (2024).
- [56] H. LaBollita, V. Pardo, M. R. Norman, and A. S. Botana, Assessing spin-density wave formation in $La_3Ni_2O_7$ from electronic structure calculations, *Phys. Rev. Mater.* **8**, L111801 (2024).
- [57] T. Kaneko, H. Sakakibara, M. Ochi, and K. Kuroki, Pair correlations in the two-orbital Hubbard ladder: Implications for superconductivity in the bilayer nickelate $La_3Ni_2O_7$, *Phys. Rev. B* **109**, 045154 (2024).
- [58] C. Lu, Z. Pan, F. Yang, and C. Wu, Interplay of two E_g orbitals in superconducting $La_3Ni_2O_7$ under pressure, *Phys. Rev. B* **110**, 094509 (2024).
- [59] S. Rye, N. Witt, and T. O. Wehling, Quenched Pair Breaking by Interlayer Correlations as a Key to Superconductivity in $La_3Ni_2O_7$, *Phys. Rev. Lett.* **133**, 096002 (2024).
- [60] H. Schlömer, U. Schollwöck, F. Grusdt, and A. Bohrdt, Superconductivity in the pressurized nickelate $La_3Ni_2O_7$ in the vicinity of a BEC–BCS crossover, *Communications Physics* **7**, 366 (2024).
- [61] J. Chen, F. Yang, and W. Li, Orbital-selective superconductivity in the pressurized bilayer nickelate $La_3Ni_2O_7$: An infinite projected entangled-pair state study, *Phys. Rev. B* **110**, L041111 (2024).
- [62] H. Liu, C. Xia, S. Zhou, and H. Chen, Role of crystal-field-splitting and long-range-hoppings on superconducting pairing symmetry of $La_3Ni_2O_7$ (2023), [arXiv:2311.07316](https://arxiv.org/abs/2311.07316) [cond-mat.supr-con].
- [63] Z. Ouyang, J.-M. Wang, J.-X. Wang, R.-Q. He, L. Huang, and Z.-Y. Lu, Hund electronic correlation in $La_3Ni_2O_7$ under high pressure, *Phys. Rev. B* **109**, 115114 (2024).
- [64] W.-X. Chang, S. Guo, Y.-Z. You, and Z.-X. Li, Fermi surface symmetric mass generation: a quantum Monte-Carlo study (2023), [arXiv:2311.09970](https://arxiv.org/abs/2311.09970) [cond-mat.str-el].
- [65] X. Sui, X. Han, H. Jin, X. Chen, L. Qiao, X. Shao, and B. Huang, Electronic properties of the bilayer nickelates $R_3Ni_2O_7$ with oxygen vacancies ($R = La$ or Ce), *Phys. Rev. B* **109**, 205156 (2024).
- [66] Y.-Y. Zheng and W. Wú, Superconductivity in the Bilayer Two-orbital Hubbard Model (2023), [arXiv:2312.03605](https://arxiv.org/abs/2312.03605) [cond-mat.str-el].
- [67] J.-R. Xue and F. Wang, Magnetism and Superconductivity in the t - J Model of $La_3Ni_2O_7$ Under Multiband Gutzwiller Approximation, *Chinese Physics Letters* **41**, 057403 (2024).
- [68] M. Kakoi, T. Kaneko, H. Sakakibara, M. Ochi, and K. Kuroki, Pair correlations of the hybridized orbitals in a ladder model for the bilayer nickelate $La_3Ni_2O_7$, *Phys. Rev. B* **109**, L201124 (2024).
- [69] Y. Shen, J. Huang, X. Qian, G.-M. Zhang, and M. Qin, Numerical study of bi-layer two-orbital model for $La_3Ni_2O_7$ on a plaquette ladder (2024), [arXiv:2411.13399](https://arxiv.org/abs/2411.13399) [cond-mat.str-el].
- [70] J. Wang and Y. feng Yang, Highly asymmetric superconducting dome and strange metallicity in $La_3Ni_2O_7$ (2024), [arXiv:2408.09774](https://arxiv.org/abs/2408.09774) [cond-mat.supr-con].
- [71] S. Hirthe, T. Chalopin, D. Bourgund, P. Bojović, A. Bohrdt, E. Demler, F. Grusdt, I. Bloch, and T. A. Hilker, Magnetically mediated hole pairing in fermionic ladders of ultracold atoms, *Nature* **613**, 463 (2023).
- [72] Z. Zhu, D. N. Sheng, and Z.-Y. Weng, Pairing versus phase coherence of doped holes in distinct quantum spin backgrounds, *Phys. Rev. B* **97**, 115144 (2018).
- [73] H.-C. Jiang, S. Chen, and Z.-Y. Weng, Critical role of the sign structure in the doped Mott insulator: Luther-Emery versus Fermi-liquid-like state in quasi-one-dimensional ladders, *Phys. Rev. B* **102**, 104512 (2020).
- [74] T. Ma, D. Wang, and C. Wu, Doping-driven antiferromagnetic insulator-superconductor transition: A quantum Monte Carlo study, *Phys. Rev. B* **106**, 054510 (2022).
- [75] S. R. White, Density matrix formulation for quantum renormalization groups, *Phys. Rev. Lett.* **69**, 2863 (1992).
- [76] U. Schollwöck, The density-matrix renormalization group in the age of matrix product states, *Ann. Phys.* **326**, 96 (2011).
- [77] A. Gleis, J.-W. Li, and J. von Delft, Controlled Bond Expansion for Density Matrix Renormalization Group Ground State Search at Single-Site Costs, *Phys. Rev. Lett.* **130**, 246402 (2023).
- [78] W. Li, S.-J. Ran, S.-S. Gong, Y. Zhao, B. Xi, F. Ye, and G. Su, Linearized Tensor Renormalization Group Algorithm for the Calculation of Thermodynamic Properties of Quantum Lattice Models, *Phys. Rev. Lett.* **106**, 127202 (2011).
- [79] B.-B. Chen, L. Chen, Z. Chen, W. Li, and A. Weichselbaum, Exponential Thermal Tensor Network Approach for Quantum Lattice Models, *Phys. Rev. X* **8**, 031082 (2018).
- [80] Q. Li, Y. Gao, Y.-Y. He, Y. Qi, B.-B. Chen, and W. Li, Tangent Space Approach for Thermal Tensor Network Simulations of the 2D Hubbard Model, *Phys. Rev. Lett.* **130**, 226502 (2023).
- [81] X.-W. Yi, Y. Meng, J.-W. Li, Z.-W. Liao, W. Li, J.-Y. You, B. Gu, and G. Su, Nature of charge density waves and metal-insulator transition in pressurized $La_3Ni_2O_7$, *Phys. Rev. B* **110**, L140508 (2024).
- [82] G. Zhou, W. Lv, H. Wang, Z. Nie, Y. Chen, Y. Li, H. Huang, W. Chen, Y. Sun, Q.-K. Xue, and Z. Chen, Ambient-pressure superconductivity onset above 40 K in bilayer nickelate ultrathin films (2024), [arXiv:2412.16622](https://arxiv.org/abs/2412.16622) [cond-mat.supr-con].
- [83] A. Weichselbaum, Non-abelian symmetries in tensor networks : A quantum symmetry space approach, *Ann. Phys.* **327**, 2972 (2012).
- [84] A. Weichselbaum, X-symbols for non-Abelian symmetries in tensor networks, *Phys. Rev. Research* **2**, 023385 (2020).
- [85] M. Fishman, S. R. White, and E. M. Stoudenmire, The ITensor Software Library for Tensor Network Calculations, *SciPost Phys. Codebases* , 4 (2022).
- [86] M. Fishman, S. R. White, and E. M. Stoudenmire, Codebase release 0.3 for ITensor, *SciPost Phys. Codebases* , 4 (2022).
- [87] G. Kresse and J. Furthmüller, Efficient iterative schemes for ab initio total-energy calculations using a plane-wave basis set, *Phys. Rev., B Condens. Matter* **54**, 11169 (1996).
- [88] A. A. Mostofi, J. R. Yates, G. Pizzi, Y.-S. Lee, I. Souza, D. Vanderbilt, and N. Marzari, An updated version of wannier90: A tool for obtaining maximally-localised Wannier functions, *Comput. Phys. Commun.* **185**, 2309 (2014).

Appendix

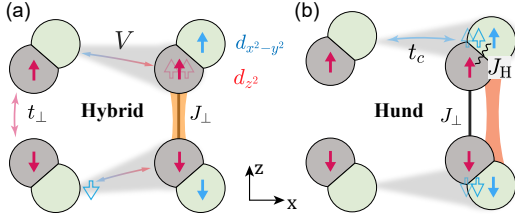


FIG. A1. Illustration of (a) hybridization dominated and (b) Hund's rule coupling dominated scenarios, which emphasizes respectively the hybridization V and Hund's rule coupling J_H plays a primary role in forming the SC order.

Hybridization versus Hund's rule coupling scenarios.— In Fig. A1, we illustrate the hybridization and Hund's SC scenarios. In the hybridization picture [Fig. A1(a)], there is a strong interlayer pairing between d_{z^2} orbitals due to the significant AF coupling J_{\perp} . The formed d_{z^2} pairs gain phase coherence through hybridization V with itinerant $d_{x^2-y^2}$ orbitals. On the other hand, a different scenario considers that the Hund's rule coupling plays the primary role. The itinerant $d_{x^2-y^2}$ band gains interlayer AF correlation through the strong on-site Hund's rule coupling that symmetrizes the spins of $d_{x^2-y^2}$ and d_{z^2} orbitals.

Ground-state and finite-temperature tensor network methods.— We exploit the density matrix renormalization group (DMRG) [75, 76] and state-of-the-art thermal tensor network methods [79, 80] to compute the zero- and finite-temperature properties, respectively. Non-Abelian and Abelian symmetries are implemented with the tensor library QSpace [83, 84] and ITensor [85, 86]. In both calculations, we consider the $2 \times L_x$ (with L_x up to 64) two-orbital ladders, and retain up to $D^* = 4500 \text{ U}(1)_{\text{charge}} \times \text{SU}(2)_{\text{spin}}$ multiplets or $D = 9000 \text{ U}(1)_{\text{charge}} \times \text{U}(1)_{\text{spin}}$ individual states in the DMRG simulations. The results are well converged with typical truncation error $\epsilon \sim 10^{-6}$. In tanTRG calculations, we consider system size 2×24 , and a small pairing field is applied to compute the pairing susceptibility. We use $\mathbb{Z}_{2,\text{charge}} \times \text{SU}(2)_{\text{spin}}$ symmetry and retain up to $D^* = 2000$ multiplets (equivalent to ~ 5200 individual states), which renders well converged results with truncation error $\epsilon \sim 10^{-4}$. The electron density can be controlled by adjusting the chemical potential term $-\mu N_{\text{tot}}$, where N_{tot} represents the total electron count. By fine-tuning the parameter μ , we ensure that the two-orbital system remains approximately at $3/8$ filling at low temperatures.

DMRG convergence.— Figure A2(a) illustrates the convergence of DMRG results, with interlayer pairing correlations from $D^* = 3000$ and $4000 \text{ U}(1)_{\text{charge}} \times \text{SU}(2)_{\text{spin}}$ multiplets showing excellent consistency up to distance $r \sim 30$. Figure A2(b) shows the exponential decay of spin correlations and single-particle Green's functions, indicating the presence of Luther-Emery SC phase. In Figs. A2(c,d) we adjust the in-

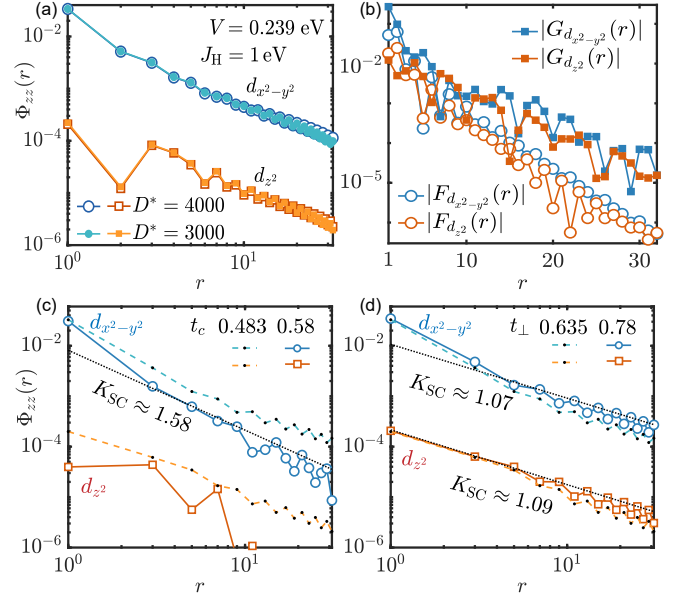


FIG. A2. (a) Interlayer pairing correlations Φ_{zz} and (b) spin correlation and single-particle Green's function are computed with $V = 0.239$ eV, $J_H = 1$ eV, where the results are well converged versus different D^* . To simulate the pressure effects, we increase (c) intralayer hopping t_c and coupling J_c , and (d) interlayer hopping t_{\perp} and coupling J_{\perp} , and find the results change only quantitatively with t_c, J_c and t_{\perp}, J_{\perp} . Here we assume $J = 4t^2/U$ with $U = 4$ eV, and fixed other model parameters at their pristine values.

tralayer $d_{x^2-y^2}$ hopping t_c and interlayer d_{z^2} hopping t_{\perp} to their realistic values in over-pressured phase (70 GPa), respectively. In both cases we find algebraically decaying Φ_{zz} which accounts for robust SC order in the ground state. Nevertheless, the enhancement of t_c as well as J_c signifies the interorbital frustration, leading to a weaker SC with $K_{SC} \approx 1.58$ for $d_{x^2-y^2}$ orbital and even absence of SC for d_{z^2} orbital. On the contrary, SC slightly benefits from the enhancement of t_{\perp} and J_{\perp} , which strengthens the interlayer AF coupling. However, the impact of these parameters on the SC order is not very prominent. In the main text, we find that the interorbital hybridization V plays an essential role in the over-pressured regime and have chosen to show related results in Fig. 4.

DFT calculations.— We use the Vienna ab initio simulation package (VASP) to optimize the lattice structure and obtain the electronic band structure [87]. The convergence criterion for atomic forces during structural optimization was set to 1 meV/Å. The total energy convergence threshold for electronic self-consistent processes was set to 10^{-8} eV/atom. A plane-wave cutoff energy of 520 eV is employed. The Γ -centered $12 \times 12 \times 12$ Monkhorst-Pack k-points grid in reciprocal space was utilized in the self-consistent cycle. The Wannier90 package is employed to downfold the band structure and construct the two-orbital model comprising Ni- $d_{x^2-y^2}$ and d_{z^2} orbitals [88]. Results obtained with various configurations are

NM (La ₃ Ni ₂ O ₇)	t_c	t_d	V	t_{\perp}	ε_c	ε_d [eV]
0 GPa	0.397	0.073	0.189	0.618	0.765	0
10	0.475	0.103	0.230	0.664	0.742	0
20	0.502	0.105	0.252	0.690	0.752	0
30	0.522	0.112	0.265	0.714	0.762	0
40	0.534	0.125	0.279	0.724	0.638	0
50	0.556	0.125	0.286	0.750	0.772	0
60	0.570	0.131	0.295	0.765	0.773	0
70	0.582	0.137	0.303	0.780	0.767	0
80	0.593	0.143	0.310	0.794	0.759	0
90	0.604	0.147	0.317	0.807	0.759	0
100	0.614	0.152	0.324	0.819	0.750	0
125	0.634	0.162	0.340	0.844	0.733	0
150	0.645	0.167	0.351	0.861	0.742	0

CDW-AF (La ₃ Ni ₂ O ₇)	t_c	t_d	V	t_{\perp}	ε_c	ε_d [eV]
0 GPa	0.124 ~ 0.178	0.025 ~ 0.068	0.088 ~ 0.192	0.549	-1.182 ~ 1.651	-1.518 ~ 1.626
30	0.069 ~ 0.239	0.077 ~ 0.084	0.163 ~ 0.242	0.666	-1.542 ~ 1.545	-1.468 ~ 1.613

NM (La ₂ PrNi ₂ O ₇)	t_c	t_d	V	t_{\perp}	ε_c	ε_d [eV]
0 GPa	0.349	0.049	0.176	0.488	0.920	0
30	0.474	0.099	0.245	0.660	0.918	0
80	0.598	0.150	0.307	0.795	0.977	0
150	0.650	0.144	0.343	0.844	0.957	0

TABLE I. Tight-binding parameters of the two-orbital model for La₃Ni₂O₇ and La₂PrNi₂O₇ determined by Wannier downfolding from DFT calculations. Non-magnetic (NM), antiferromagnetic (AF) and charge density wave (CDW) configurations are considered. Calculations at low pressures (0 and 10 GPa) are based on the *Amam* orthorhombic phase, whereas the *I4/mmm* tetragonal phase is used for calculations at high pressures (≥ 20 GPa).

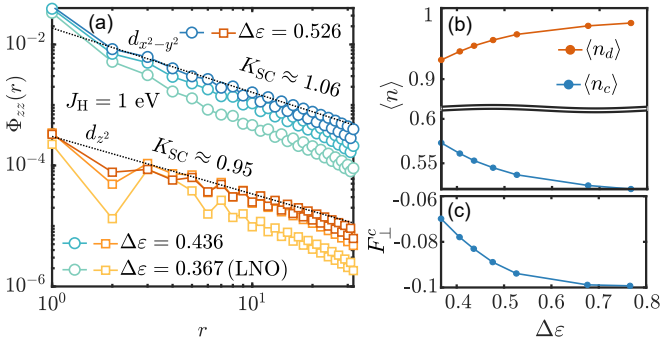


FIG. A3. (a) Interlayer pairing correlations of both the $d_{x^2-y^2}$ and d_{z^2} orbitals with different site energy offsets $\Delta\varepsilon \equiv \varepsilon_c - \varepsilon_d$. $\Delta\varepsilon = 0.367$ eV is estimated from DFT calculations on La₃Ni₂O₇ under about 30 GPa pressure [20]. We artificially increase $\Delta\varepsilon$ between the two e_g orbitals, and compute (b) the electron densities and (c) interlayer spin correlation F_{\perp}^c .

summarized in Tables. I. For the CDW-AF phase, the oxygen octahedra exhibit in-plane distortions, and Ni atoms can occupy two inequivalent sites. Consequently, the parameters like hybridization V and hopping t_c exhibit spatial distributions, represented by the error bars in the table and also in Fig. 4(a)

of the main text. There are two inequivalent Wyckoff positions for La atoms in La₂PrNi₂O₇. It is found that Pr doping at the La2 position (inside the NiO bilayer) has lower energy, as low as 593.3 meV/f.u. for *Amam* phase and 437.9 meV/f.u. for *I4/mmm* phase. Note that in all calculations, low-pressure data (0 and 10 GPa) are obtained from *Amam* orthorhombic phase while high-pressure results are from *I4/mmm* tetragonal phase.

Site energy and enhanced superconductivity.— In Fig. A3 we increase the difference in the site energies between the two orbitals. As $\Delta\varepsilon$ increases, more electrons are transferred to the d_{z^2} orbital while keeping $n_e = 3/8$. Other realistic parameters remains unchanged [20]. In Fig. A3(a) we show that the pairing correlations of both orbitals are significantly enhanced with increasing $\Delta\varepsilon$. The resulting electron densities, $\langle n_c \rangle$ for the $d_{x^2-y^2}$ orbital and $\langle n_d \rangle$ for the d_{z^2} orbital, are shown in Fig. A3(b). As the d_{z^2} orbital approaches half-filling (thus containing fewer holes), a stronger interlayer AF correlation F_{\perp}^c can be observed between the $d_{x^2-y^2}$ orbitals, as illustrated in Fig. A3(c). This provides insights into potential experimental strategies for achieving higher critical temperature T_c or stabilizing the SC order in ambient conditions.